Experimental and Numerical Study of a New Dynamic Phenomenon for Two-bladed Wind Turbines

Larsen, Torben J.; Kim, Taeseong

Published in:
International Offshore and Polar Engineering Conference. Proceedings

Publication date:
2015

Document Version
Publisher's PDF, also known as Version of record

Proceedings of the Twenty-fifth (2015) International Ocean and Polar Engineering Conference **www.isope.org**
Kona, Big Island, Hawaii, USA, June 21-26, 2015

ISBN 978-1-880653-89-0; ISSN 1098-6189

Experimental and Numerical Study of a New Dynamic Phenomenon for Two-bladed Wind Turbines

Torben Juul Larsen and Taeseong Kim**
Department of Wind Energy, Technical University of Denmark
Roskilde, Denmark

*The two authors contributed equally to this work

ABSTRACT

In this paper the dynamics of a two-bladed turbine is investigated numerically as well as experimentally with respect to how the turbine frequencies change with the rotor speed. It is shown how the turbine frequencies of a two-bladed rotor change with the azimuthal position at standstill and how the frequencies start whirling during rotor rotation. The whirling for two-bladed rotors change with multiple P contributions and not only ±1P as is previously seen for three-bladed wind turbine rotors. A three-bladed turbine was also analyzed in similar way and results were compared. This turbine was investigated both in a perfect isotropic condition where all blades have identical properties as well as an imbalanced edition where one blade had increased mass.

KEY WORDS: Wind turbine; Dynamics; Experiment; Imbalanced rotor; Campbell; Whirling; Two blades; Three blades.

INTRODUCTION

In the search for more cost-effective wind energy, two-bladed turbines seem to have gained a renewed interest. This is exemplified by the new 3.6MW size of two-bladed offshore wind turbine with partial pitched blades by Envision. A prototype of this turbine has been erected at Thyborøn in Denmark, where it has been tested since September 2012. One of the main drivers for this concept is a potential to reduce extreme tower bottom loads in storm situations by up to 60% compared with a similar three-bladed wind turbine. For both two- and three-bladed turbines it is of utmost importance to be able to predict the structural frequencies at both standstill and operation as significantly increased vibration levels can occur if an unfortunate resonance between the load input frequencies and a low damped structural vibration mode occurs. In a previous study (Kim *et al*., 2014) loads and dynamics were compared between a two- and three-bladed configuration based on numerical simulations. From this study it was observed that the rotor whirl mode frequencies change differently with respect to rotor speed for two- and three-bladed rotors, respectively. For both concepts, the frequency of asymmetric rotor modes change mainly with the rotor speed (±1P) which is well known with respect to three-bladed turbines and rotors in general (Hansen, 2007) (Swanson, 2005). However for the two-bladed rotor, the split in frequencies differed from the normal disc behavior as the whirl modes frequencies split up with not just ±1P, but also multiple P frequencies, see Fig 1. The explanation is that the two-bladed rotor has asymmetric properties depending on the azimuth angle as the global rotor inertia and therefore the global standstill turbine frequencies differ with respect to the azimuth angle. This was first observed in the numerical studies in (Kim *et al*., 2014), where it was also seen that a tower frequency component ±2P is present. As these results have so far only been observed in numerical studies, an experimental study has now also been performed, in order to validate the previous numerically derived conclusions. An experimental model turbine has been produced with structural properties directly scaled from the full scale 3.6MW turbine using the method of Froude scaling (Jaint *et al*, 2012). The natural frequencies are compared between the full and the scaled turbine with good agreement.

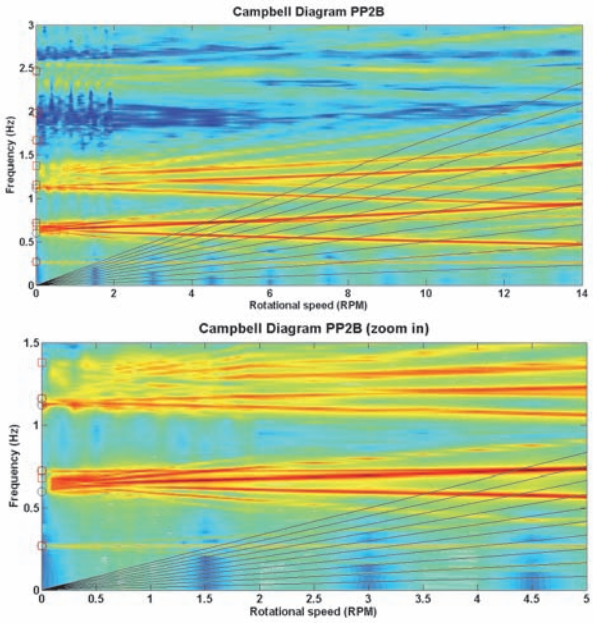

Fig 1. Numerical results from (Kim *et al.*, 2014). Campbell diagram of turbine frequencies during rotation for the two-bladed 3.6MW Envision turbine. Whirl modes are split with 1, 2, …, nP. Top: Full overview. Bottom, zoom view at lowest frequencies.

TEST TURBINE CONFIGURATION AND EXPERIMENTAL SETUP

A downscaled model of the 3.6MW Envision turbine was created. As the point of interest is mainly on the structural dynamics, the aerodynamic properties were configured to create as small impact as possible. The structural properties was scaled based on Froude scaling where the ratio between gravity and inertial loads are kept constant (Jaint *et al.*, 2012). Furthermore, the design was simplified from a practical point of view. The most essential part was the placement of the lowest turbine frequencies at standstill, and that the structural damping was as low as possible. The natural frequencies of the full scaled turbine, Froude scaled turbine (target frequency), and the numerical model used in this study are shown in Table 1.

Table 1. Natural frequency comparisons (target versus simulated frequency).

Mode	Full size turbine	Target (1:75)	Actual (1:75) (simulated)
1st tower	0.23Hz	1.99Hz	2.09 Hz
1st flap	0.69 Hz	5.98Hz	6.1 Hz
1st edge	1.08 Hz	9.35Hz	9.85 Hz

The final design consisted of blades made of simple prismatic aluminum bars of the dimension 5×8mm. The rotor diameter is 1640 mm. The tower was made out of a circular aluminum bar with a height of 1600mm and a diameter of 16mm. In order to fulfill the Froude scaling, the nacelle properties had to be with a low weight and it was decided to use a gearmotor also as the load carrying part of the nacelle. As the gearmotor was DC connected, the rotor speed could be varied from 0-150rpm by varying the voltage over the motor with a linear relation. A special aluminum mounting block was created, where the rotor tower distance could be varied. The hub was also made as a simple aluminum structure to which the blades were mounted with simple screw connections, see Fig. 2. Due to the layout pattern of the mounting holes on the hub disc the turbine could be easily changed from two-bladed to three-bladed configuration, see Fig 1.

Fig. 3 shows the two- and three-bladed configuration used for the measurements.

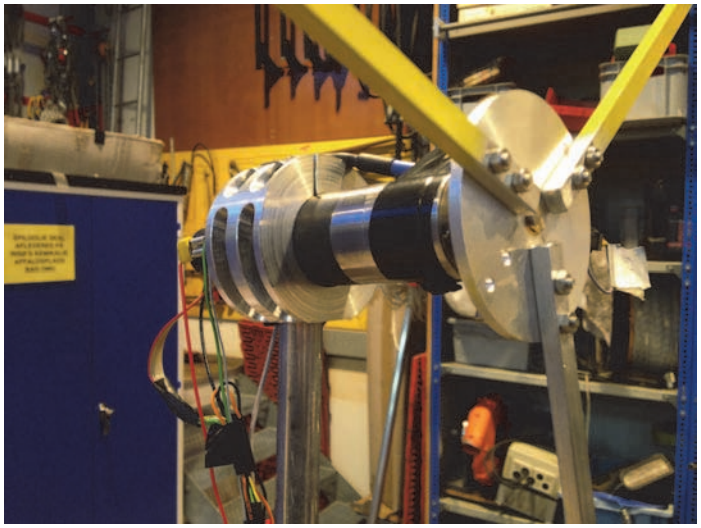

Fig. 2: Nacelle and hub configuration of the turbine configured with three blades.

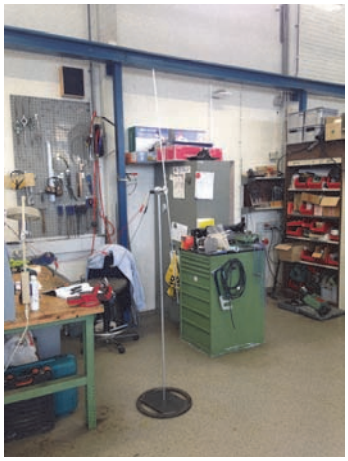

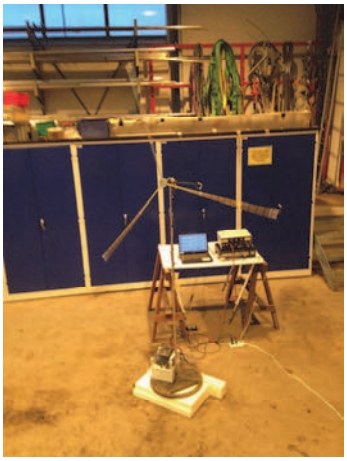

Fig. 3: Model turbine in two-bladed configuration (left) and three-bladed configuration (right).

The blades were created in a simple way using aluminum bars with a rectangular cross section with dimensions 5×8 mm. In this way, it was ensured that the ratio between flap- and edgewise frequency agreed with the target values shown in Table 1. However, during the first test runs it was seen that the turbine was instable with respect to flapwise blade vibrations even for rather modest rotor speeds. The reason for these vibrations was most likely vortex induced vibration caused by the rectangular aerodynamic shape. To destroy the coherent vortex structure it was decided to twist a wire around the blades. This seemed to be a very efficient solution and the blades were therefore configured with wires in all the experiments, see Fig. 4. The diameter of the wire was 1mm.

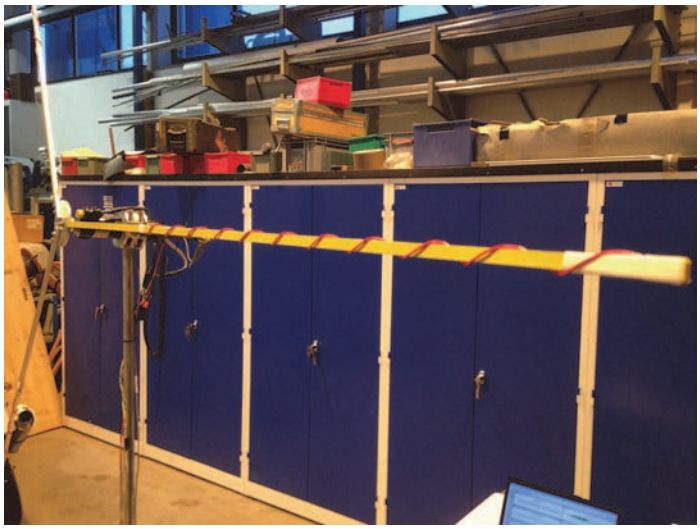

Fig. 4: Wire wound on the blades.

In one of the experiments, the three-bladed rotor was configured with a mass imbalance on one of the blades. The extra weight was 14g corresponding to 15% of the blade weight, mounted at 50% radius, see Fig. 5. The presence of the added weight will to some extent also increase the aerodynamic damping, but it has not been possible to quantify the amount.

The vibration accelerations were measured with four Brüel and Kjaer Type 4507B accelerometers connected to a Type 3560C front end receiver. The accelerometers were mounted mid on the tower in height 1000mm measuring tower fore-after and side-side accelerations. One accelerometer was mounted in the tower top at height 1600mm measuring side-side accelerations. The last accelerometer was mounted on a carbon fiber boom pointing sideways of the tower/gear motor assembly in a lateral distance of 150mm from the tower center line. The direction of this accelerometer was in the fore-after direction measuring contributions from fore-after motions together with yaw motion contributions.

Fig. 5: A simple mount of an extra weight on one blade.

Fig. 6: Accelerometer mounting at the mid tower.

The vibration modes of the turbine during standstill and rotation were excited with impulse excitation using a simple manual hammering using a pencil. For each measurement period the turbine was excited using four impacts on the blades in both flap and edgewise direction and at two different azimuthal locations on the spinning rotor.

In the experiment with the mass-imbalanced three-bladed rotor, the maximum rotor speed was 90rpm corresponding to just below resonance between 1P and 1st tower mode. The tower vibrations at this point was approximately ±20cm making it too dangerous to continue.

NUMERICAL METHOD

The study in this paper is based on numerical analysis using the aeroelastic software HAWC2, developed at DTU Wind Energy. The structural part of the code is a multibody formulation based on the floating frame of reference method as described in (Larsen and Hansen, 2012) and (Kim *et al.*, 2013). In the particular formulation of the code, the turbine structure is subdivided into a number of bodies, where each body has its own coordinate system. Within each body, the structure consists of an assembly of linear Timoshenko beam elements. The nonlinear effects of the body motion (rotations and deformations) are accounted for in the coupling constraints in between the individual bodies. Small deflections are assumed within the linear beam elements. This means that effects of large rotations and deflections are included using a proper subdivision of a blade to a number of bodies. As only the structural part of the code has been used for this study the detailed descriptions of the aerodynamic parts are described in (Madsen *et al*., 2012), (Larsen *et al*., 2013) and (Kim *et al.*, 2014). The code verification has been performed through the Offshore Code Comparison Collaboration (OC3) and Offshore Code Comparison Collaboration Continuation (OC4) under the International Energy Agency (IEA) Wind Task where HAWC2 results are validated against other numerical tools such as BLADED, ADAMS, FAST, FLEX and so on (Popko *et al*., 2012) and (Vorpahl *et al*., 2013). The full system natural frequencies, dynamic loads and displacements are compared in OC3 and OC4. From the comparisons, it has been shown that the full system natural frequencies and the dynamic loads and responses obtained by HAWC2 agree well with other aeroelastic codes. A full-scale validation of simulated and measured wind turbine load levels have recently been presented in (Larsen *et al.*, 2013).

NUMERICAL RESULTS

The downscaled turbine (1:75) was modeled in the simulation code, HAWC2, and the standstill eigenfrequencies of the two- and three-bladed turbine were calculated, see Table 2. What is important to notice is that the standstill eigenfrequencies of the turbine differ depending on the rotor azimuthal position. The tower frequencies are slightly lower when the rotor is vertical than horizontal, mainly caused by the different rotor inertia around the pitch axis and the two perpendicular axis. The asymmetric flap mode differs significantly between the two positions, which is mainly caused by the difference in flapwise stiffness of the nacelle. In the horizontal configuration the flapwise motion couples to the tower torsion, whereas in the vertical configuration the flapwise motion couples to the second tower mode with increased stiffness. The same occurs for the edgewise frequency where the edgewise motion couples with the for-aft tower mode (and shaft tilt bending) in the horizontal mode and couples with the side-side tower motion (and tower torsion) in the vertical configuration. In between the modes in horizontal and vertical configuration, the eigenfrequencies varies with a sinusoidal variation.

Table 2. Standstill turbine frequencies, simulated.

Mode	Two bladed Horizontal	Two bladed Vertical
1st tower transverse	2.09 Hz	2.07 Hz
1st tower for-aft	2.11 Hz	2.08 Hz
1st asym flap	4.79 Hz	5.84 Hz
1st sym flap	6.63 Hz	6.69 Hz
1st asym edge	8.52 Hz	8.47 Hz
1st sym edge	9.80 Hz	10.47 Hz

The variation of standstill frequencies as function of azimuth position is shown in Fig. 7. Here it is clearly seen that the asymmetric rotor flap and symmetric rotor edge mode differ significantly as function of azimuth angle.

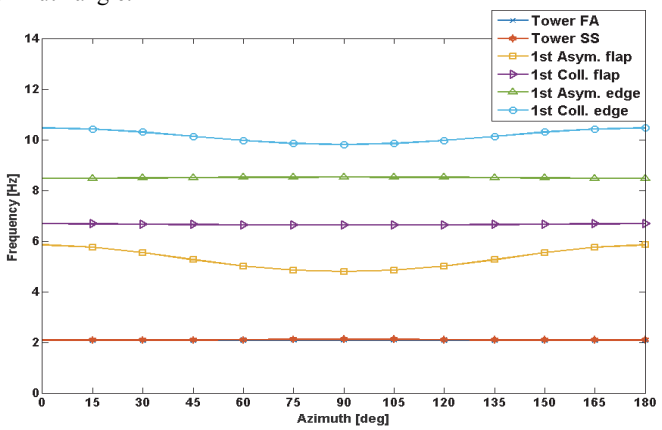

Fig. 7: Natural frequency variations with respect to the rotor azimuth angle.

The model has also been investigated with respect to how the natural frequencies change as function of rotor speed. This was done based on impulse excitation of the turbine modes in time domain assuming no aerodynamic forces present. In total 6 different excitations are applied where the middle of the blade in flap and edgewise directions, the tower top in fore-aft and side-side directions, the blade root in positive edgewise direction and the middle of the blade in negative edgewise direction at the same time, and the blade root in positive flapwise direction and the middle of the blade in the negative flapwise direction at the same time are excited. The results are presented in Fig. 8, where a Campbell diagram has been created based on the response seen in the tower top yaw moment. The tower frequency at 2Hz, which is the straight line, is clearly seen and so are the whirling components of the tower motion at the tower base frequency ±2P, which are the angled lines. At zero rpm, the asymmetric flapwise frequencies between 4.2 and 5Hz can be seen. A lot of frequencies seem to be present in the area, which is explained by the azimuthal dependency. Furthermore, whirling components of the asymmetric flapwise base frequency of 4.2Hz±2P, and looking close it is also possible to see a 4.2Hz+4P component. The symmetric flapwise mode also has whirl components at 6.6Hz±1P and ±2P and even the asymmetric edgewise mode at 8.5Hz show this behavior. From this figure it is also possible to see higher harmonics of the forward tower whirl component at f_0+nf_0+2P, with f_0 being the base tower frequency and n = 1,..,8. These higher harmonics of the tower forward whirling are probably a result of the impulsive excitation approach which is commonly known to excite higher harmonics of eigenfrequencies. A special thing to remark is that the whirl modes originated from the asymmetric flap and edge modes also includes a central component with a frequency that is constant with respect to rotor speed variation. The cause for this component is so far unclear.

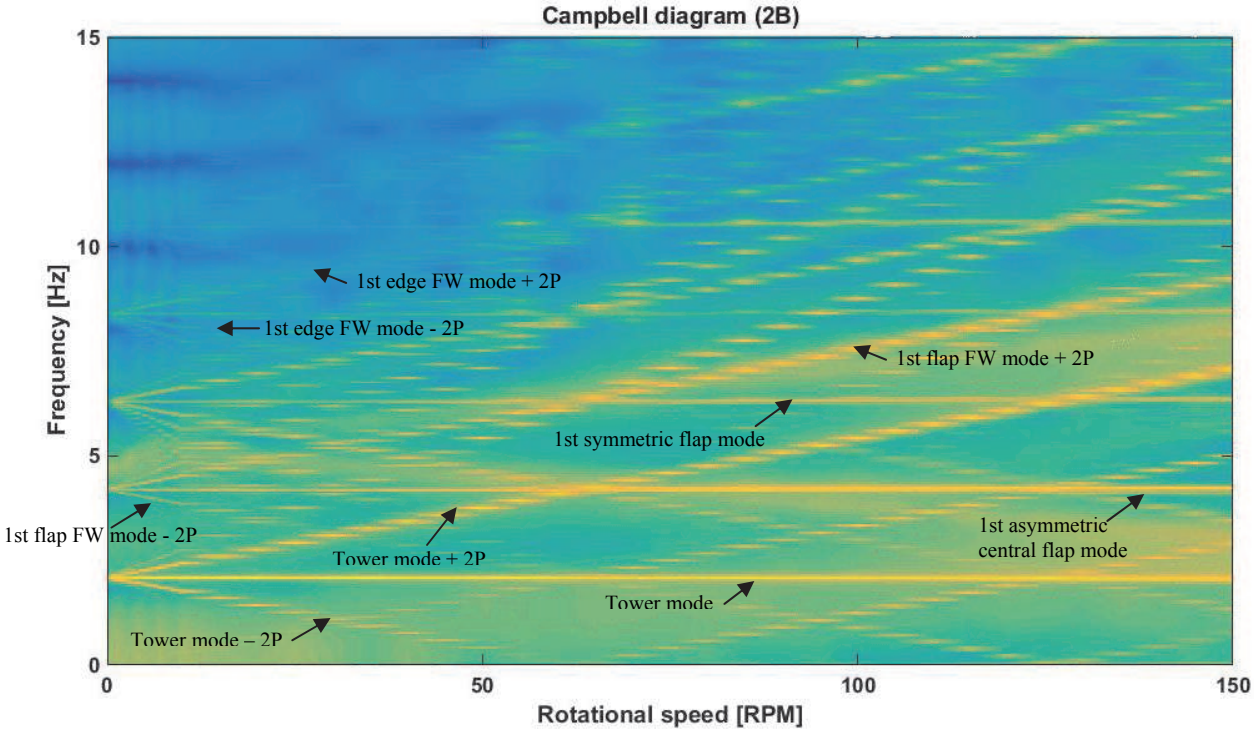

Fig. 8: Campbell diagram for simulated response of the 2B turbine during impulsive excitation of the model scale turbine.

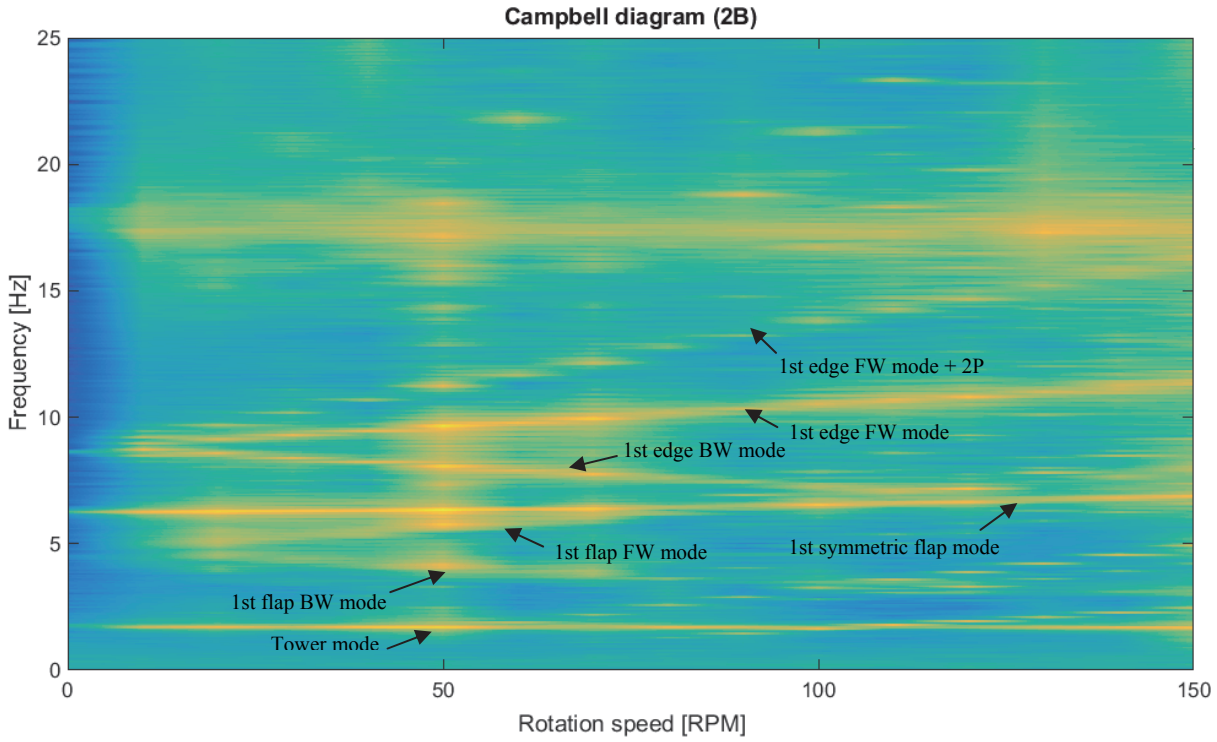

Fig. 9: Campbell diagram of the eigenfrequencies measured for the two- bladed configuration.

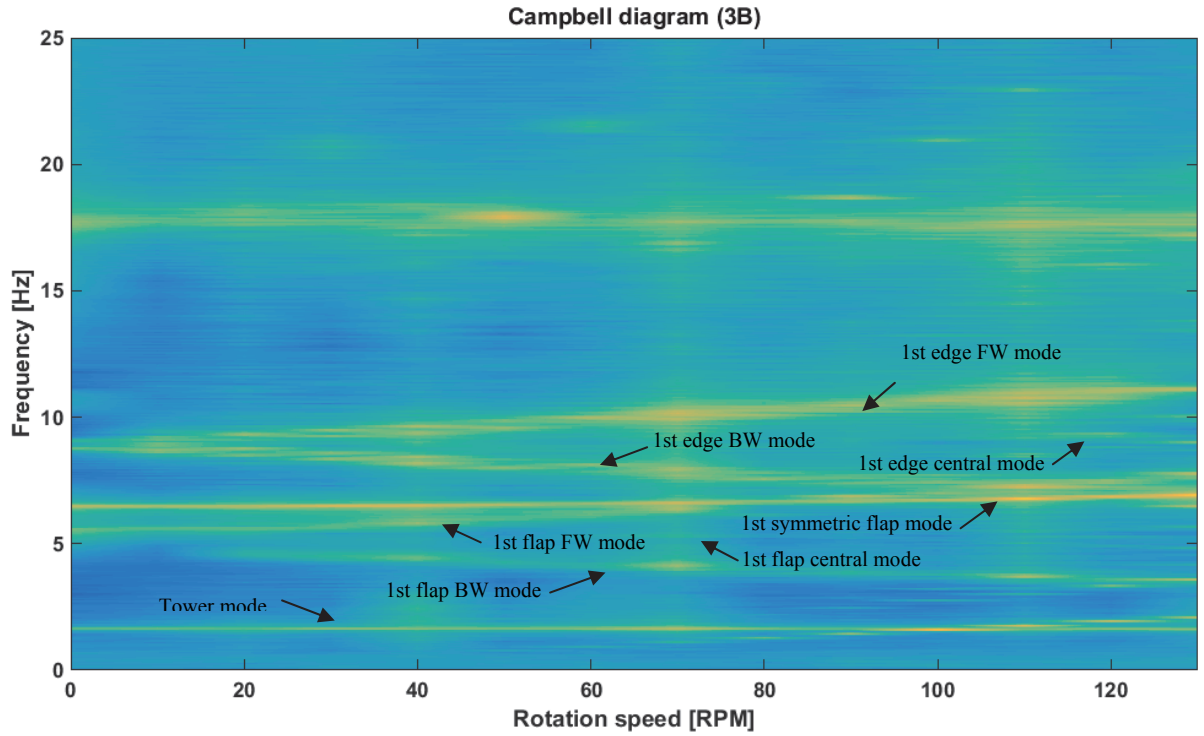

Fig. 10: Campbell diagram of the eigenfrequencies measured for the three-bladed configuration.

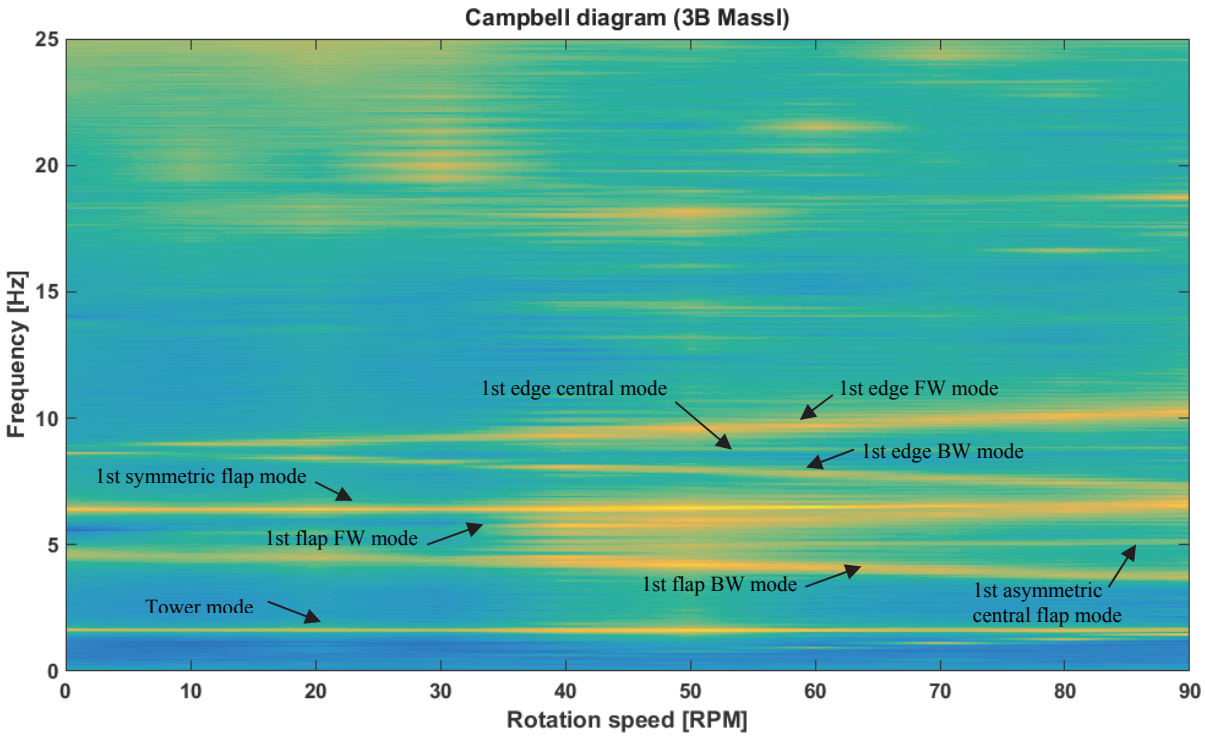

Fig. 11: Campbell diagram of the eigenfrequencies measured for the mass imbalanced three-bladed configuration

EXPERIMENTAL RESULTS

Experiments were carried out for a two-bladed, a three-bladed configuration and a three-bladed mass imbalanced configuration. In all cases Campbell diagrams were created, see Fig. 9~11.

From Fig. 9 it can be seen that the tower frequency at 2Hz is constant for all rotor speeds. The symmetric flap mode at 6.6Hz has a slight increase caused by the centrifugal stiffening. What is especially interesting to notice is that the measurements confirms that the asymmetric flapwise and the symmetric edgewise rotor modes splits into whirl mode with a ±1P split. Secondly, it is also very interesting to notice that the whirl modes also has component of multiple P's. Especially the edgewise mode +2P is clearly visible. The plot is not as clear with respect to the flapwise whirling (it is because the flapwise mode is aerodynamically damped), but it is possible to see that this also has components of ±2P.

The three-bladed rotor also has modes that split into whirl modes, see Fig. 10. These whirl modes has it basis in the asymmetric flap and edge modes at standstill. When the rotor increases rotational speed these modes split into the well-known forward and backward whirl modes separated with ±1P. There are no presences of multiple P components in the whirl modes.

As the difference in whirl mode behavior, perhaps, can be explained by the two-bladed rotor being highly asymmetric with respect to inertial properties, an extra experiment was carried out. Here the three-bladed rotor was configured with an extra mass on one of the blades. In this configuration the rotor is also non-isotropic. The results are presented in Fig. 11. From this figure it is only possible to see the same whirl mode frequencies as for the isotropic configuration. The numerical findings about a non-isotropic three bladed rotor having whirl mode components with multiple P components can therefore not be confirmed by this experiment. It is also clearly visible that central flap and edge modes exist in the imbalance case. These frequencies are constant with respect to the rotational speed. These modes can to some extent also be seen in the experiment of the balanced three bladed turbine, however the magnitude is small. As this should theoretically not be present for a perfectly isotropic rotor, it could indicate that the experimental turbine is not perfectly isotropic due to manufacturing and mounting tolerances.

CONCLUSIONS

With this study based on both numerical and experimental investigations we conclude the following:

- The asymmetric rotor modes, seen in a global frame of reference, will for a two-bladed turbine at standstill and during slow rotation vary with the azimuth position of the rotor.
- When the rotor speed is increased, the asymmetric rotor modes of a two-bladed turbine will split into a pair of whirl modes. The frequency of these whirl modes starts as the standstill frequency (averaged over all azimuth angles) and one will increase with 1P (forward whirl mode) and one will decrease with 1P (backward whirl mode). Furthermore, the impact of centrifugal stiffening will cause a general increase of all rotor modes, which in the present experiment is a minor contribution.
- The whirl modes of a two-bladed rotor not only split with ±1P, but also with multiple P. This has so far only been seen in numerical studies, but is now experimentally verified. In the numerical simulations it was clear that multiple P frequencies can be present. In the experiment it was only possible to excite the ±1P and ±2P frequencies. Even though this potential makes it difficult to design a two-bladed rotor without presence of resonance, the multiple P

contributions appear to be difficult to excite and hence have less vibration levels than the ±1P whirl modes.

- The presence of whirl modes for a three-bladed turbine has been confirmed. The frequency of the rotor whirl modes splits with ±1P with base frequency in the asymmetric rotor modes at standstill.
- For an imbalanced three bladed rotor, a center frequency whirl component is seen in the experiment. This was also seen in the simulations of the two bladed turbine, but could so far not be seen in the experiment of the two bladed configuration.

If a three-bladed turbine is not isotropic, it was expected that the whirl modes will have multiple P contributions (as a two-bladed rotor) because of the asymmetric rotor inertia caused by the mass imbalance. The magnitude of these higher components are however small in magnitude and it was not possible to validate this finding in the experimental results. Detailed numerical and experimental investigations with the three-bladed mass imbalance rotor will be investigated in future work.

ACKNOWLEDGEMENTS

This work is funded by the EUDP-2011 II project Demonstration of Partial Pitch 2-Bladed Wind Turbine Performance and the International Collaborative Energy Technology R&D Program of the Korea Institute of Energy Technology Evaluation and Planning (KETEP), granted financial resource from the Ministry of Trade, Industry & Energy (No. 20138520021140), which are gratefully acknowledged.

REFERENCES

Hansen, MH, Gaunaa, M, and Madsen, HA (2004). "A Beddoes–Leishman type dynamic stall model in state-space and indicial formulations," *Technical Report Risø-R-1354(EN)*, Risø National Laboratory.

Hansen, MH (2007). "Aeroelastic instability problems for wind turbines," *Wind Energy*, 10, 551–577.

Jaint, A, Robertson, AN, Jonkman, JM, Goupee, AJ, Kimball, RW, Swift, AHP (2012). "*FAST Code Verification of Scaling Laws for DeepCwind Floating Wind System Tests*." *22nd International Offshore and Polar Engineering Conference*, Rhodes, Greece, ISOPE, Vol 1.

Kim, T, Hansen, AM, and Branner, K (2013). "Development of an anisotropic beam finite element for composite wind turbine blades in multibody system," *Renewable Energy*, 59, 172-183.

Kim, T, Larsen, TJ, and Yde, A (2014). "Investigation of potential extreme load reduction for a two-bladed upwind turbine with partial pitch," *Wind Energy,* doi: 10.1002/we.1766.

Larsen, TJ, and Hansen, AM (2012). "How to HAWC2, the user's manual," *Technical Report Risø-R-1597(ver.4-3) (EN)*, DTU Wind Energy, Roskilde, Denmark.

Larsen, TJ, Madsen, HA, Larsen, G, and Hansen, KS (2013). "Validation of the Dynamic Wake Meander Model for Loads and Power Production in the Egmond aan Zee Wind Farm," *Wind Energy*, 16, 605–624.

Leishman, JG, and Beddoes, TS (1986). "A generalized model for airfoil unsteady aerodynamic behaviour and dynamic stall using the indicial method," *Proc. of the 42nd Annual Forum of the American Helicopter Society*, Washington D.C., June 2-5, 1986.

Madsen, HA, Riziotis, V, Zahle, F, Hansen, MOL, Snel, H, Grasso, F, Larsen, TJ, Politis, E, and Rasmussen, F (2012). "Blade element momentum modeling of inflow with shear in comparison with advanced model results," *Wind Energy*, 15, 63–81.

Madsen, HA, Riziotis, V, Zahle, F, Hansen, MOL, Snel, H, Grasso, F, Larsen, TJ, Politis, E, and Rasmussen, F (2011). "BEM blade element momentum modeling of inflow with shear in comparison with advanced model results," *Wind Energy,* 15, 63–81.

Popko, W, Vorpahl, F, Zuga, A, Kohlmeier, M, Jonkman, J, Robertson, A, Larsen, TJ, Yde, A, Sætertrø, K, Okstad, KM, Nichols, J, Nygaard, TA, Gao, Z, Manolas, D, Kim, K, Yu, Q, Shi, W, Park, H, Vásquez-Rojas, A, Dubois, J, Kaufer, D, Thomassen, P, de Ruiter, MJ, Peeringa, JM, Zhiwen, H, von Waaden, H (2012). "Offshore code comparison collaboration continuation (OC4) phase I —results of coupled simulations of an offshore wind turbine with jacket support structure," *Journal of Ocean and Wind Energy*, ISOPE, 1(1), 1-11: Also in *Proceedings of the 22nd International Society of Offshore and Polar Engineers Conference*, Rhodes, Greece, ISOPE, Vol 1.

Swanson, E, Powel, CD, and Weissman, S (2005). "A practical review of rotating machinery critical speeds and modes," *Sound and Vibration*, 10-17.

Theodorsen, T (1935). "General theory of aerodynamic instability and the mechanism of flutter," *NACA Report 435*, 413–433.

Vorpahl, F, Strobel, M, Jonkman, JM, Larsen, TJ, Passon, P, Nichols, J (2013). "Verification of aero-elastic offshore wind turbine design codes under IEA wind task XXIII," *Wind Energy,* DOI:10.1002/we.1588.